Universality in effective conductivity of regular 2D and 3D composites

V Sh Machavariani

School of Physics and Astronomy, Raymond and Beverly Sackler Faculty of Exact Sciences, Tel-Aviv University, 69978 Tel-Aviv, Israel

Abstract
We have found that for variety of composite materials there is a domain of universal behaviour of the effective conductivity σ_{eff}. This domain can be qualitatively characterized as a range of 'low contrast' of the components ($0.2 \leqslant \sigma_1/\sigma_2 \leqslant 5$). In the domain of the universality the equation $\sigma_{\text{eff}} \approx \exp(\sum n_i \ln \sigma_i)$ gives a good approximation for σ_{eff} of all the investigated regular structures (2D and 3D composites, two and three component composites, isotropic and anisotropic composites, composites with equal and different concentrations of components) as well for random random media (ZBLAN20 glass-forming melt). Equally these results are valid for the thermal conductivity and diffusivity of the composite media.

1. Introduction

Earlier we studied both physical [1] and mathematical [2] (include a review of the problem) features of regular symmetric composites. In this paper we generalize our consideration to the case of anisotropic and non-symmetric composites. We have found that for a variety of composite materials there is a domain of a universal behaviour of the effective conductivity σ_{eff}. This domain can be qualitatively characterized as a range of 'low contrast' of the components. For this domain of the universality we suggest a formula which gives a very good approximation for the effective conductivities of all the investigated structures. Equally these results are valid for the thermal conductivity and diffusivity of the composite media.

In section 2 we consider the qualitive foundation for the suggested 'universal' formula. In section 3 we test it for the variety of regular composite structures (two dimensional (2D) and three dimensional (3D) composites, two and three component composites, isotropic and anisotropic composites, composites with equal and different concentration of components— see figure 1). In section 4 we check up the suggested formula for random media using experimental conductivity and density data on ZBLAN20 ($0.53ZrF_4$–$0.20BaF_2$–$0.04LaF_3$–$0.03AlF_3$–$0.20NaF$, [3]) glass-forming liquid. Conclusions are presented in section 5.
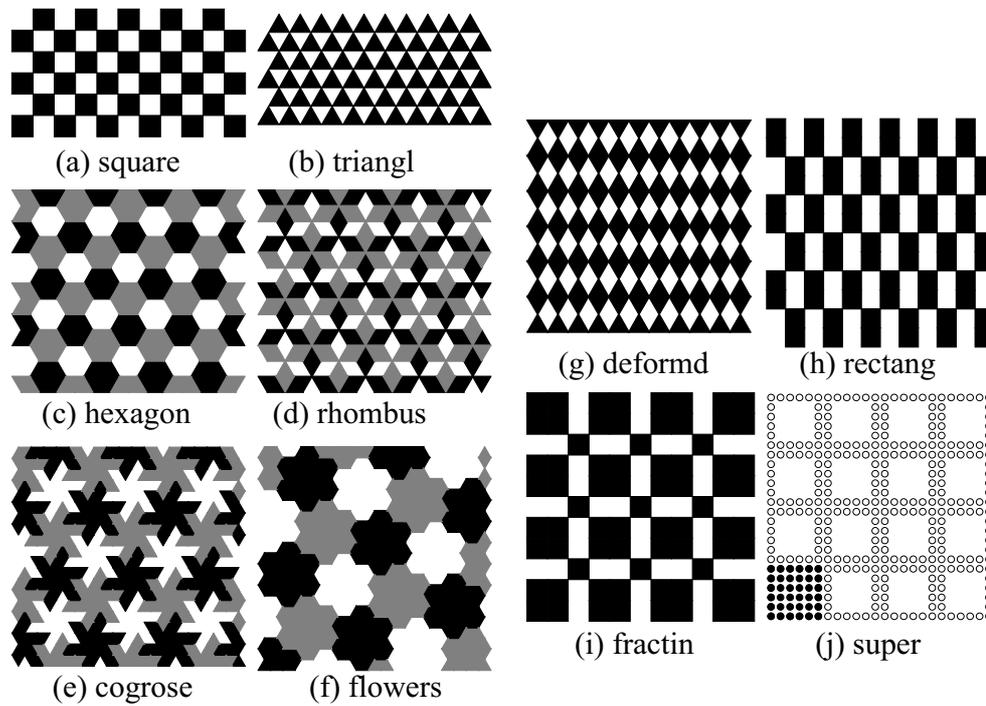
Figure 1. 2D regular isotropic and anisotropic structures investigated in the present work. Captions denote the nickname of the computer code.

2. Qualitative foundation

In 1970 Dykhne [4] found an exact analytical solution for the effective conductivity σ_{eff} of a 2D checker board (figure 1(a)).

$$\sigma_{\text{eff}} = \sqrt{\sigma_1 \sigma_2} \tag{1}$$

where σ_1 and σ_2 are the conductivities of the white and black squares respectively. The result of equation (1) is equally valid for a triangular 2D lattice (figure 1(b)) and any random isotropic distribution of black and white spots of arbitrary shape until their surface concentrations are equal.

Let us consider the infinite 2D checker board whereby 'black' and 'white' squares of this board are not uniform. Let the 'white' squares be in their turn checker boards (not infinite) of 'green' and 'blue' squares (with conductivities σ_1 and σ_2 respectively); and let the 'black' squares be checker boards (not infinite) of 'red' and 'yellow' squares (with conductivities σ_3 and σ_4 respectively). In this case $\sigma_1 \approx \sqrt{\sigma_1 \sigma_2}$, $\sigma_2 \approx \sqrt{\sigma_3 \sigma_4}$ and $\sigma_{\text{eff}} \approx \sqrt[4]{\sigma_1 \sigma_2 \sigma_3 \sigma_4}$.

This construction is illustrated in figure 2(a). Instead of the sign 'equal' we have used 'approximately equal' because of the finite (not infinite) size of 'blue–green' and 'red–yellow' checker boards. The larger the number of squares in these boards, the more accurate the equations are. Such a construction physically corresponds to the presence of different length scales: medium range order, short range order etc.

Repeating this construction a number of times leads to the following expression:

$$\sigma_{\text{eff}} \approx \sigma_1^{n_1} \sigma_2^{n_2} \cdots \sigma_i^{n_i} \cdots \tag{2}$$
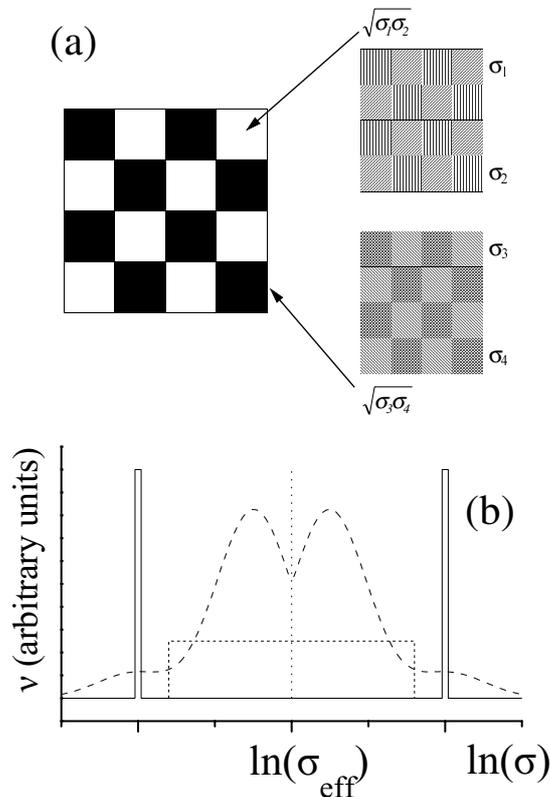
Figure 2. (a) Schematic illustration of the multi-disperse model. The white and black squares of the left checker board are not homogeneous. They in their turn are also checker boards (right part). (b) Schematic presentation of the probability density of the local conductivity for validity of equation (3) in the 2D case.

where n_i is the concentration of components. For figure 2(a) all n_i are equal to $1/4$. But if some of the σ_i are equal to each other, different values for n_i follow. The analogous consideration is valid for a triangular lattice or a random isotropic distribution of arbitrary spots.

Let us look at a similar problem: the conductivity of the surface $\sigma = \sigma(x, y)$ depends smoothly on the local coordinates (x, y). In this case $\nu(\sigma)\Delta\sigma$ is the probability of the conductivity at the arbitrary point to be within the interval from σ to $\sigma + \Delta\sigma$. It has been shown by Dykhne [4] that the exact expression for the effective conductivity is going to be given by

$$\ln \sigma_{\mathrm{eff}} = \int \nu(\sigma)\mathrm{d}(\ln \sigma) \tag{3}$$

under conditions that the effective conductivity of the infinite surface is isotropic and the probability density ν as a function of $\ln \sigma$ is symmetric. Figure 2(b) presents schematically some of the possible cases. Solid bars correspond to the case of a two coloured square, triangular or random array of spots. The dashed curves correspond to the cases of some smooth conductivity distributions. Tortet *et al* [5] have successfully used the rectangular distribution (figure 2(b), dotted lines) of the active part of the conductivity to describe the impedance data on composite ('brushite') material.

Both cases (see equations (2) and (3)) give the same dependence for the effective conductivity σ_{eff}. Therefore, one can introduce the interpolation formula σ_0 for the effective conductivity $\sigma_{\text{eff}} \approx \sigma_0$:

$$\sigma_0 = \exp\left(\sum_i n_i \ln \sigma_i\right) \tag{4}$$

where n_i is the surface or volume fraction of the ith component; σ_i is the conductivity of the ith component.

In the next sections we investigate the domain of validity of equation (4). We show that this equation gives a very good approximation for the effective conductivity in the case of small difference between the partial conductivities (further on we will call it the 'low contrast of conductivities' domain).

3. Regular composites

In this section we perform the numerical calculation of the effective conductivity for the following regular structures: (i) 2D three colour isotropic schemes with the ratio of the fractions being equal to 1:1:1 (figures 1(c), 1(d), 1(e) and 1(f)); (ii) 2D two colour anisotropic schemes with the ratio of the fractions being equal to 1:1 (figures 1(g) and 1(h)); (iii) 2D two colour isotropic schemes with the ratio of the fractions being equal to $n : m$ (figure 1(i)); (iv) 3D two colour isotropic schemes with the ratio of the fractions being equal to 1:1. The 2D two colour square and triangular checker boards (figures 1(a) and 1(b)) were used as a test case.

In section 3.1 the 2D structures are considered. The numerical algorithm is described in section 3.1.1, the isotropic and anisotropic structures are considered in sections 3.1.2 and 3.1.3, respectively. Section 3.1.4 treats the isotropic structures with different concentration of the components. Finally, section 3.2 presents our results for a 3D checker board.

3.1. 2D composites

3.1.1. Numerical algorithm. The algorithm approximates the system of materially continuous squares (or triangles) by a square (or correspondingly, triangular) network of conducting wires. Each square (or triangle) is divided into M^2 equal cells. The centre of each cell is connected to the centres of four (or three) of the nearest neighbouring cells by conducting wires. The resistance of the wire connecting the ith and jth cells is equal to $\frac{\sigma_i + \sigma_j}{A \sigma_i \sigma_j}$, where σ_i and σ_j are the conductivities of the ith and jth cells respectively, M is the number of grid points in the edge of each square (or triangle) and the coefficient $A = 2$ for the square lattice and $A = 2\sqrt{3}$ for the triangular one. Translational symmetry of the problem has been taken into account by choosing the periodical boundary condition for currents. The symmetry planes (where they exist) of the problem have been taken into account to reduce the computational time for solving the system of N linear algebraic equations. In the case of square or triangular checker boards (figures 1(a) and 1(b)) $N = 2M^2$; all the other structures were constructed from equal triangles or squares. For example, for the `hexagon` structure (figure 1(c)) $N = 18M^2$.

To achieve higher accuracy we have implemented the following algorithm of calculation. This algorithm is schematically illustrated in figure 1(j). Centers of the circles correspond to the centres of the cubcells. Let us consider first the isolated object α (small square or triangle; solid circles in figure 1(j)). The number of edge subcells is N_{surface} while the number of internal subcells is N_{bulk}. The total number of subcells $N_{\text{all}} = N_{\text{surf}} + N_{\text{bulk}} = n^2$. The voltage in the

centre of the ith edge subcell is V_i, and the voltage in the centre of the jth bulk subcell is $\tilde{U}_j$. One can solve the system of $N_{\text{all}}N_{\text{bulk}}$ equations and express $\tilde{U}_j$ via U_i in the form

$$\tilde{U}_j = \sum_{i=1}^{N_{\text{surf}}} A_{ji} U_i \qquad j = 1, 2, \ldots, N_{\text{bulk}}. \tag{5}$$

Using matrix A_{ij} one can express the current I_i which come from outside the object into the ith edge subcells in the form

$$I_i = \sum_{i=1}^{N_{\text{surf}}} B_{ij} U_j \qquad j = 1, 2, \ldots, N_{\text{surf}}. \tag{6}$$

In the next step we construct the object β (open circles in figure 1(j)) from the object α for which we know the dependence of equation (6). Therefore in this step we do not consider the internal subcells of the object α and drastically reduce the number of equations to be solved.

This procedure can be repeated several times to obtain the maximal efficiency. In the computer code developed the small square (or triangle) is used to construct the middle ones. The middle square in its turn is used to calculate the matrix from equation (6) for the big one. The big square (or triangle) is used to construct the subpart of the colour schemes, for example the hexagon, and the hexagon is used to construct the colour scheme presented in figure 1(c). To calculate the effective conductivity for another set of σ_1, σ_2 and σ_3 one does not need to repeat all the procedure, one needs to repeat only the last step.

Using this step-by-step algorithm we have achieved the maximal efficiency. This means that the size of the program is kept minimal as well as computation time. The efficiency of this algorithm compared with the traditional one is tested in the case of the program which allocates operative memory which is necessary to keep the matrix of 2500×2500 equations (50 MByte). The optimized code use exactly the same size of memory. This algorithm allows us to increase the number of grid points by 50–200 times (with about the same computation time).

3.1.2. Isotropic n-colour case. Comparison of the numerical results for square and triangular checker boards (figures 1(a) and 1(b)) with the exact [4] solution shows that our computational algorithm gives an effective conductivity Σ^N which monotonically approaches (for $N \to \infty$) to the exact value of conductivity from below, e.g., $\delta\sigma \to 0$ for $N \to \infty$. Here $\delta\sigma(N) = \sigma_{\text{eff}} - \Sigma^N$ is a deviation of the numerical lower bound from the exact solution. Moreover, the dependence of $\delta\sigma(N)$ on N has a linear form in a log–log plot. This means that $\delta\sigma$ can be presented in the following form:

$$\delta\sigma(N) = \frac{\alpha}{N^\beta}. \tag{7}$$

To find the upper bound we have used the consequence of *duality* of the 2D problem [6]:

$$\sigma_{\text{eff}}(\sigma_1^{-1}, \sigma_2^{-1}, \ldots, \sigma_n^{-1})\sigma_{\text{eff}}(\sigma_1, \sigma_2, \ldots, \sigma_n) = 1 \tag{8}$$

Our algorithm being applied directly to the problem with conductivities $1/\sigma_1$, $1/\sigma_2$ and $1/\sigma_3$ gives the lower bound for the value $1/\sigma_{\text{eff}}$ and thus the upper bound for the value σ_{eff} itself. Thus

$$\sigma^{(-)}(N) = \Sigma^N(\sigma_1, \sigma_2, \sigma_3, \ldots) \qquad \sigma^{(+)}(N) = 1/\Sigma^N\left(\frac{1}{\sigma_1}, \frac{1}{\sigma_2}, \frac{1}{\sigma_3}, \ldots\right) \tag{9}$$

where $\sigma^{(-)}$ and $\sigma^{(+)}$ are the lower and the upper bounds respectively, Σ^N is the numerical result for the number N of subcells. These bounds are independent because the deviation from

the exact solution which originates from the changing of the continuous case on the network, is different for different values of σ_1, σ_2 and σ_3.

The results of calculation for isotropic 2D three component composites (hexagon— figure 1(c), rhombus—figure 1(d), cogrose—figure 1(e)—and flowers—figure 1(f)) are presented in figure 3(a). While both upper and lower boundaries are presented, sometimes it is difficult to distinguish them because of a very high accuracy of the calculation. The coordinates of point O are $(\sigma_1, \sigma_2, \sigma_3) = (0.001, 0.001, 1)$, point A has the coordinates $(0.5, 0.5, 1)$, point B has the coordinates $(0.999, 0.001, 1)$ (for directions OB and AB) or $(1, 0.001, 1)$ (for a direction CB) and point C has the coordinates $(1, 1, 1)$. Let us note here that the knowledge of σ_{eff} for all the points within the triangle OBC (strictly speaking, for the values $0 \leqslant \sigma_1 \leqslant 1, 0 \leqslant \sigma_2 \leqslant \sigma_1$, $\sigma_3 = 1$) solve the problem for all the possible values of $(\sigma_1, \sigma_2, \sigma_3)$. Indeed, because of invariancy to permutations, we can rearrange and rename the conductivities in such a manner that $\sigma_2 \leqslant \sigma_1 \leqslant \sigma_3$. Using the property of the homogeneity of the first order one obtains:

$$\sigma_{\text{eff}} = \sigma_{\text{eff}}(\sigma_1, \sigma_2, \sigma_3) = \sigma_3 \sigma_{\text{eff}}(\sigma_1/\sigma_3, \sigma_2/\sigma_3, 1) \tag{10}$$

where $0 \leqslant \sigma_1/\sigma_3 \leqslant 1, 0 \leqslant \sigma_2/\sigma_3 \leqslant \sigma_1/\sigma_3$, and $1 = 1$.

One can see from figure 3(a) that near the points O, A and C the effective conductivities for different structures are practically coincide. The universal behaviour of σ_{eff} can be easily seen from figure 3(b), which presents the $\sigma_{\text{eff}}/\sigma_0$ ratio. One can clearly see that near the points O, A and C the simple formula for σ_0 describes very well ($\sigma_{\text{eff}}/\sigma_0 \approx 1$) the effective conductivity for all the investigated structures. The points A and C can be characterized qualitatively as points of 'low contrast'. This means that the different structures behave universally if the contrast between the properties of the component is small. The exact meaning of the word 'small' depends on the accuracy we are looking for. The shadowed area in figure 4 schematically presents the area of the universal behaviour. At the same time, this area corresponds to the area of validity of equation (4).

3.1.3. Anisotropic two colour case. To find the upper bound in the case of a two colour anisotropic sample (figures 1(g) and 1(h)) we have used Keller's result [6]. Thus, the lower ($\sigma_{xx}^{(-)}$ and $\sigma_{yy}^{(-)}$) and upper ($\sigma_{xx}^{(+)}$ and $\sigma_{yy}^{(+)}$) bounds for the exact principal values have the form

$$\sigma_{xx}^{(-)}(N) = \Sigma_{xx}^{N}(\sigma_1, \sigma_2) \qquad \sigma_{xx}^{(+)}(N) = \sigma_1\sigma_2/\Sigma_{yy}^{N}(\sigma_2, \sigma_1) \tag{11}$$

$$\sigma_{yy}^{(-)}(N) = \Sigma_{yy}^{N}(\sigma_1, \sigma_2) \qquad \sigma_{yy}^{(+)}(N) = \sigma_1\sigma_2/\Sigma_{xx}^{N}(\sigma_2, \sigma_1). \tag{12}$$

To analyse the results for anisotropic structures, let us introduce the following notations:

$$f(\sigma_1/\sigma_2) = \sigma_{yy}(\sigma_1, \sigma_2)/\sigma_0. \tag{13}$$

To describe the conductivity tensor for all the values of σ_1 and σ_2 one needs to know the value of $f(\gamma)$ function for $0 \leqslant \gamma \leqslant 1$ only, where $\gamma = \sigma_1/\sigma_2$. Indeed, using the symmetry relation one obtains

$$\text{for } \sigma_1 \leqslant \sigma_2 \qquad \begin{cases} \sigma_{xx} = \sqrt{\sigma_1\sigma_2}/f(\sigma_1/\sigma_2) \\ \sigma_{yy} = \sqrt{\sigma_1\sigma_2}f(\sigma_1/\sigma_2) \end{cases} \tag{14}$$

$$\text{for } \sigma_1 \geqslant \sigma_2 \qquad \begin{cases} \sigma_{xx} = \sqrt{\sigma_1\sigma_2}/f(\sigma_2/\sigma_1) \\ \sigma_{yy} = \sqrt{\sigma_1\sigma_2}f(\sigma_2/\sigma_1). \end{cases} \tag{15}$$

Thus, $f_{xx}(\gamma) = 1/f(\gamma)$ and $f_{yy}(\gamma) = f(\gamma)$ show the relative deviations of the σ_{xx} and σ_{yy}, respectively, from the isotropic case. Figure 5(a) presents the calculated lower and upper bounds for f_{xx} and f_{yy} for the rectang structure with $N_y : N_x = 20 : 1$. The solid line corresponds to the isotropic case. Here N_x and N_y are the lengths of the edges of the rectangle
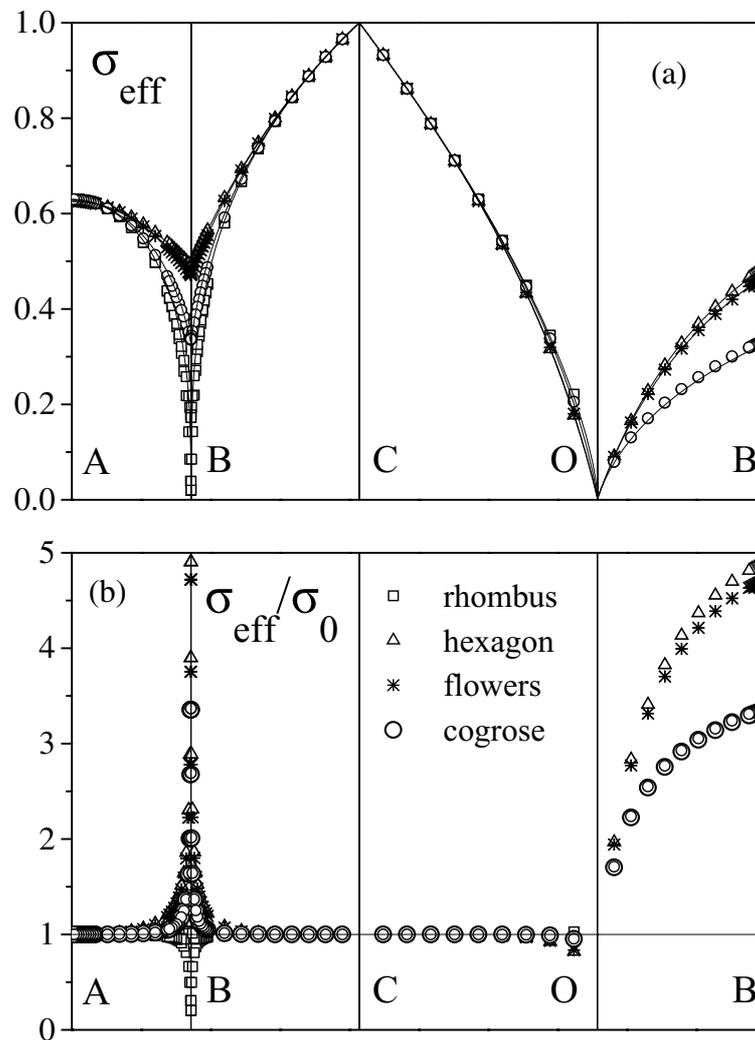
Figure 3. (a) Lower and upper bounds of the calculated effective conductivity for `hexagon`, `rhombus`, `cogrose` and `flowers` structures. In the figure the bounds coincide on the figure because of the high accuracy of the calculation. Curves are added to lead the eye. (b) Ratio $\sigma_{\text{eff}}/\sigma_0$. The straight line corresponds to $\sigma_{\text{eff}} = \sigma_0$.

(see figure 1(h) and table 1) in Ox and Oy directions, respectively. Figure 5(b) shows the deviation from isotropic behaviour $(f(\gamma) - 1)$ for the `rectang` structure with different ratios $\varepsilon = N_y/N_x$ as well as for the `deformd` structure. The curves in figure 5(b) are (from lower to upper curves) `deformed`, `rectang` with $\varepsilon = 1.333, 1.5, 1.667, 2, 2.5, 3, 3.5, 4, 5, 6, 7, 8, 10, 15$ and 20. Here $f(\gamma) = (f_{\min} + f_{\max})/2$ and $f_{\min}$ and $f_{\max}$ are the calculated lower and upper bounds for $f(\gamma)$. The function $f(\gamma, \varepsilon)$ for the values of $\varepsilon < 1$ can be obtained from the following equation:

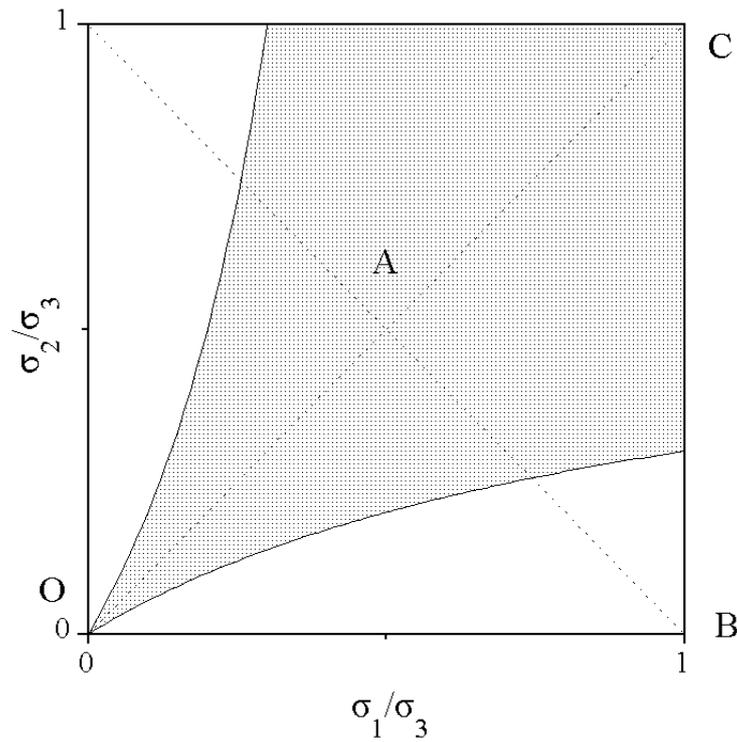$$f(\gamma, \varepsilon) = 1/f(\gamma, 1/\varepsilon). \tag{16}$$

Figure 4. The schematic view of the area (grey) of the universal behaviour of σ_{eff} for 2D three component regular composites.

Table 1. The maximal number of grid points used in the calculations with optimization for different structures and geometries.

Structure	$N_{\max}$	N_x	N_y	rectang $N_{\max}$	fractin $N_{\max}$	N_x	N_y	rectang $N_{\max}$
hexagon	952 200	1	2	345 744	166 464	1	20	51 840
rhombus	238 050	1	3	290 400	97 344	2	3	164 268
cogrose	78 408	1	4	236 672	62 500	2	5	98 000
flowers	232 974	1	5	196 000	44 100	2	7	72 828
squares	236 672	1	6	164 268	33 124	3	4	80 736
triangl	320 000	1	7	145 656	25 600	3	5	66 270
deformd	640 000	1	8	129 600	20 736			
		1	10	103 680	14 641			
		1	15	69 120	6 400			

3.1.4. Isotropic two colour case with different concentrations of the components. To find the upper bound in the case of isotropic sample but with different fractions of components (see figure 1(i)) one obtains from [6] the following expressions for the lower and upper limits $\sigma^{(-)}(N)$ and $\sigma^{(+)}(N)$:

$$\sigma^{(-)}(N) = \Sigma^N(\sigma_1, \sigma_2) \qquad \sigma^{(+)}(N) = \sigma_1\sigma_2 / \Sigma^N(\sigma_2, \sigma_1). \tag{17}$$
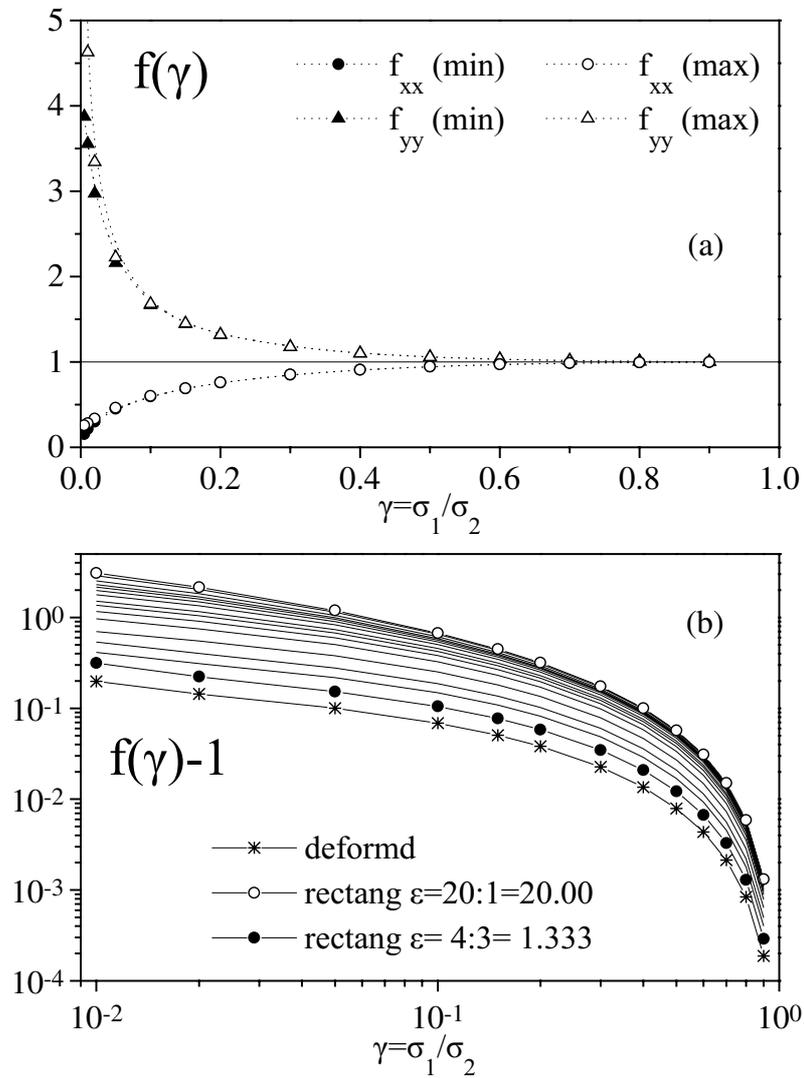
Figure 5. (a) Calculated lower and upper bounds for f_{xx} and f_{yy} in the `rectang` structure with $N_y : N_x = 20 : 1$. The solid curve corresponds to the isotropic checker board. Curves are added to lead the eye. (b) Deviation from the isotropic case $f(\gamma) - 1$ for the `rectang` structure for different ratios $\varepsilon = N_y/N_x$ as well as for the `deformd` structure. Curves are added to lead the eye.

To analyse the results for structures with different concentrations of the components, let us introduce the following notations:

$$f(\sigma_1/\sigma_2) = \sigma_{\text{eff}}/\sigma_0(\sigma_1, \sigma_2) \tag{18}$$

where n_1 and n_2 are the concentrations of the first and second components, respectively. The first component is the small square with the edge N_x and the large square with the edge N_y; the second component is two equal rectangles with edges N_x and N_y (see figure 1(i) and table 1).

$$n_1 = \frac{N_x^2 + N_y^2}{(N_x + N_y)^2} \qquad n_2 = \frac{2N_x N_y}{(N_x + N_y)^2}. \tag{19}$$

To describe the conductivity for all the values of σ_1 and σ_2 one needs to know the value of the $f(\gamma)$ function for $0 \leqslant \gamma \leqslant 1$ only. Indeed, using the symmetry relation one obtains

$$\text{for } \sigma_1 \leqslant \sigma_2 \qquad \sigma_{\text{eff}} = \sigma_1^{n_1} \sigma_2^{n_2} f(\sigma_1/\sigma_2) \tag{20}$$

$$\text{for } \sigma_1 \geqslant \sigma_2 \qquad \sigma_{\text{eff}} = \sigma_1^{n_1} \sigma_2^{n_2} / f(\sigma_2/\sigma_1). \tag{21}$$

Figure 6(a) presents the calculated lower and upper bounds for $f(\gamma)$ for the `fractin` structure with $n_1 = 0.802$. The solid line corresponds to the usual checker board with $n_1 = n_2 = 0.5$. Figure 6(b) shows the deviation from the equi-partioned case $[1 - f(\gamma)]$ for the `fractin` structure for different concentrations $n_1 = 0.556, 0.625, 0.680, 0.722, 0.755,$ $0.781, 0.802$ and 0.835. Here $f(\gamma) = (f_{\min} + f_{\max})/2$, $f_{\min}$ and $f_{\max}$ are the calculated lower and upper bounds for $f(\gamma)$.

Figures 3, 5 and 6 show that for the deviation from equation (4) is small within the range of 'low contrast' of the components ($0.2 \leqslant \sigma_1/\sigma_2 \leqslant 5$). One can also see from figures 5 and 6 that the deviation itself from the isotropic and equi-partioned cases also looks to be similar for different ε and n_1. We hope that this similarity will stimulate further investigations of the analytical properties of the regular composite materials.

3.2. 3D composite

The calculation algorithm can easily be generalized for the case of the 3D cubic checker board. The only difference now is that the number of cells in each cube is M^3; the number of nearest neighbours is 6, the number of equations is $N = 2M^3$ and the resistance of the wire between the centres of the ith and jth cells is $M \frac{\sigma_i + \sigma_j}{2\sigma_i \sigma_j}$. The maximal number of N used in our calculation is 13 718.

We found that the deviation of the numerical result for the 2D square checker board from the exact solution $\delta\sigma(N)$ can be presented according to equation (7). If one assumes the same kind of dependence to be valid for the 3D checker board, one can estimate σ_∞ from the equation

$$\sigma_\infty - \sigma_{\text{calc}}(N) = \alpha'/N^{\beta'} \tag{22}$$

where σ_∞ is an extrapolated limit of the numerical solution for an infinite number of equations. In figure 7(a) it is evident that the reasonable choice of σ_∞ values allows us to present the deviation $\sigma_\infty - \sigma_{\text{calc}}(N)$ this way (linear form in a log–log plot) in the whole range of our calculations (in three decades).

The exponent index β' (convergency factor) in equation (22) depends on the ratio of the partial conductivities γ. For $\sigma_1 \approx \sigma_2$ and $\gamma \approx 1$ ('low contrast'), the exponent β' is large (see figure 7(b)) and the convergency is fast. This means that even rough 3D grid gives a good approximation to the current distribution. In other words, a small difference in the component geometry has a very small effect on the total effective conductivity. In the case of large difference between the partial conductivities, e.g., $\gamma \ll 1$ or $\gamma \gg 1$ ('high contrast'), the exponent β' is small (see figure 7(b)). In this case the convergency is slow because a very fine grid only allows us to describe well the current distribution. Therefore the sensitivity to the components' geometry increases with the increase of the difference in partial conductivities. Let us note here that the exponent β' depends on 'conductivity contrast' the same way in the case of 2D 3-component composite. The lowest value of β' is for the `rhombus` structure for $\sigma_1 \to 0$ and $\sigma_2 \approx \sigma_3 \neq 0$. The highest value of β' is for the `hexagon` structure and $\sigma_1 \approx \sigma_2 \approx \sigma_3$.

Figure 8(a) presents the σ_∞ values (circles) for the 3D case in comparison with the exact solution for the 2D case (dashed curve) as a function of $\gamma = \sigma_1/\sigma_2$. Figure 8(b) presents the
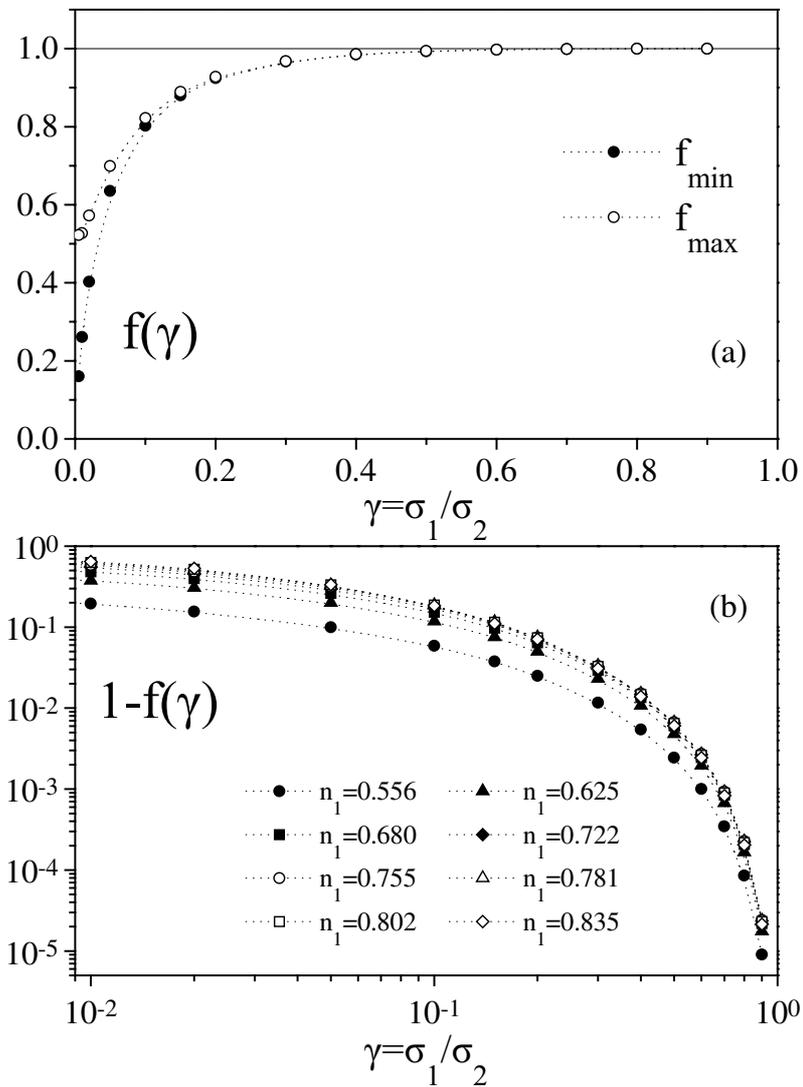
Figure 6. (a) Calculated lower (solid circles) and upper (open circles) bounds for $f(\gamma)$ in the `fractin` structure with $n_1 = 0.802$. The solid line corresponds to $n_1 = n_2 = 0.5$. Curves are added to lead the eye. (b) Deviation from the equi-partioned case $1 - f(\gamma)$ for the `fractin` structure for different concentration ratio of the first component n_1. Curves are added to lead the eye.

ratio $f(\gamma) = \sigma_{\text{eff}}/\sigma_0$, where $f(\gamma)$ is a function which expresses the above mentioned deviation between 3D and 2D cases. Because of the symmetry relation $f(\gamma) = f(1/\gamma)$ one needs to calculate the function $f(\gamma)$ only for γ from 0 to 1. It was shown [7] that its asymptotic values are $f(0) = 2$, $f(1) = 1$.

It is amazing to find out how close this 3D calculation is to the 2D case for the σ_1/σ_2 not close to zero (see figure 8). Nevertheless it might be expected since a single layer of cubes behaves exactly as a 2D checker board. Thus, the difference between 2D and 3D appears as a result of layer interconnection only. In the 3D case $\sigma_\infty \geqslant \sqrt{\sigma_1 \sigma_2}$ is in agreement with the result of [8].
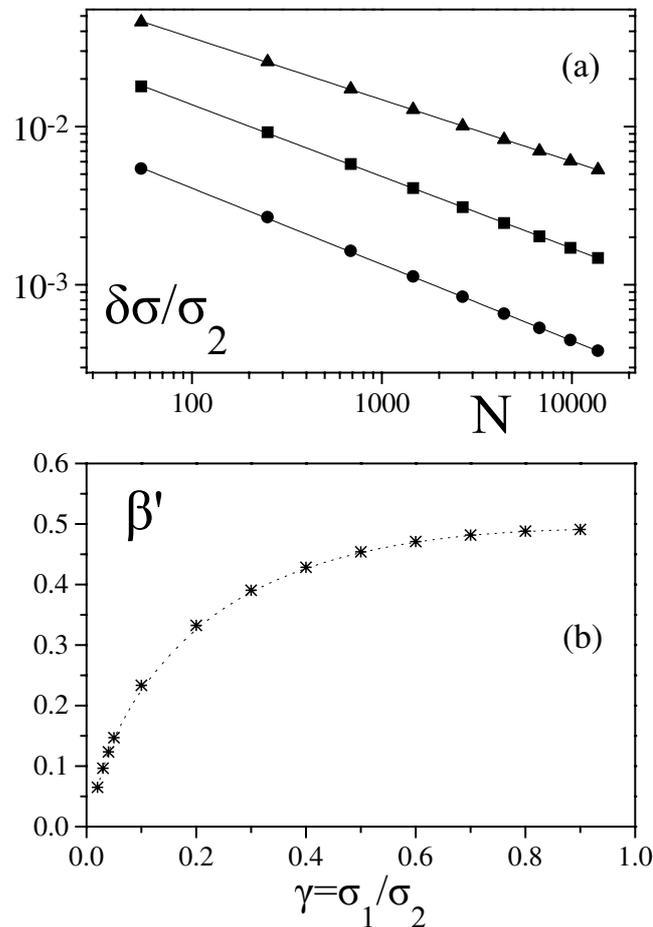
Figure 7. (a) Deviation of the numerical result from the limiting value σ_∞ for a 3D checker board as a function of the number of equations for different values of γ. Triangles correspond to the case of $\gamma = 0.3$, squares to $\gamma = 0.5$ and circles to $\gamma = 0.7$. (b) Exponent index β' (convergency factor) for a 3D checker board. Convergency decreases for $\gamma \to 0$.

4. Random composite media

In this section we consider a case of random distribution of the components. Unfortunately, the present calculation algorithm cannot be applied for the random structures. In the case of non-periodic structures the number of grid points $N \propto n^3 k^3$ (and the computation time, respectively) inceases tremendously, where n is a number of grid points in the edge of one domain, k is a number of quasi-random domains in the edge of one regular cell.

To test the validity of equation (4) in the random media we explore the experimental conductivity and density data of the ZBLAN20 ($0.53ZrF_4$–$0.20BaF_2$–$0.04LaF_3$–$0.03AlF_3$–$0.20NaF$, [3]) glassformer. Using equation (4) we estimate the concentration of the rigid phase n_{rigid} as a function of temperature [1] and compare it with n_{rigid} obtained from the temperature dependence of ZBLAN20 density. The agreement of these two independent experimental results gives a valuable justification for equation (4) in the case of random media. Let us note here that in glass-forming liquids the the ratio of the partial conductivities (e.g., 'rigid' and
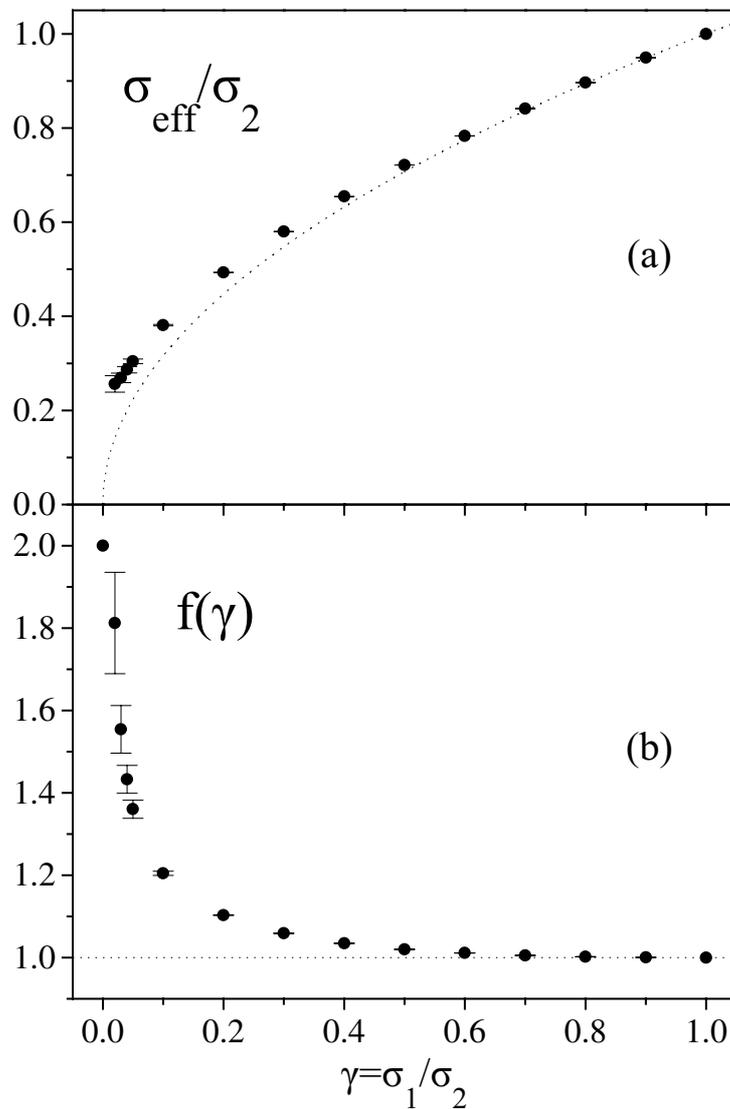
Figure 8. (a) Calculated effective conductivity for 3D (circles) and 2D (dashed curve) checker boards as a function of $\gamma = \sigma_1/\sigma_2$. The dashed curve corresponds to the 2D case. (b) The deviation function $f(\gamma) = \sigma_{\text{eff}}/\sigma_0$. The straight line corresponds to the 2D case.

'fluid' phases) might be very large. Thus for random isotropic media the domain of validity of equation (4) might be even wider than for regular composites.

The supercooled melt has been considered by many recent theories [9] as a sort of dynamically heterogeneous medium. Whatever the reason for the emergence of this heterogeneity, the corresponding liquid on its nanometric scale can be presented as a composite material with inclusions of greater rigidity (and probably of a higher density) [10, 11] which live much longer than a reorientation time of an individual molecule [11]. Actually there is, probably, a whole spectrum of local conductivities in glassifying liquid. But let us consider for the sake of simplicity a glassformer in its nanometric scale being a mixture
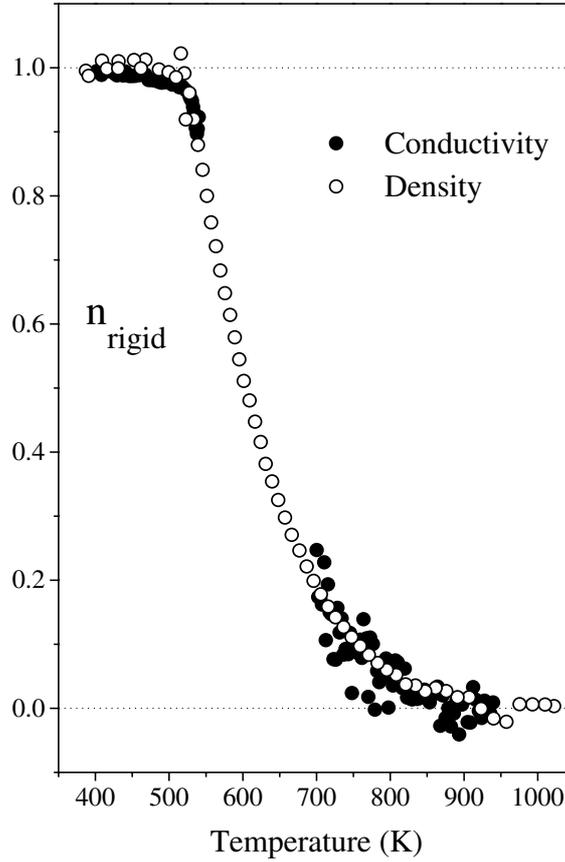
Figure 9. The calculated volume fraction n_{rigid} of the rigid clusters in ZBLAN20 glass-forming melts as a function of the temperature. Solid circles are obtained from the density data; open circles correspond to the resistivity data.

of two components only. The first component is the 'fluid-like' one with the conductivity σ_{fluid} and the volume fraction n_{fluid}. The conductivity for this component may be extrapolated from a high temperature region (Arrhenius [12, 13] behaviour) of the corresponding glassformer: $\sigma_{\text{fluid}} = \frac{A_{\text{fluid}}}{T} \exp(\frac{E_{\text{fluid}}}{T})$, where T is a temperature, E_{fluid} is an activation energy of the liquid state (in Kelvin) and A_{fluid} is a material dependent constant. The second component consists of the 'rigid-like' clusters of random form and size with conductivity σ_{rigid} and volume fraction $n_{\text{rigid}} = 1 - n_{\text{rigid}}$, where σ_{rigid} can be extracted from the glass behaviour below the glassification temperature T_g in an analogous way: $\sigma_{\text{rigid}} = \frac{A_{\text{rigid}}}{T} \exp(\frac{E_{\text{rigid}}}{T})$. Here E_{rigid} is the activation energy in the glassy state.

The volume fraction of the solid component n_{rigid} can be obtained from the the equation (4) and the extrapolated values of σ_{rigid} and σ_{fluid} as follows:

$$n_{\text{rigid}}(T) \approx \frac{\ln \sigma_{\text{fluid}}(T) - \ln \sigma_{\text{eff}}(T)}{\ln \sigma_{\text{fluid}}(T) - \ln \sigma_{\text{rigid}}(T)}. \tag{23}$$

Another way to estimate n_{rigid} is to use the density data. In both liquid and glassy states the density is roughly a linear function of the temperature. If one assumes the density of both 'rigid-like' inclusions d_{rigid} and 'fluid-like' medium d_{fluid} to be equal to the extrapolated values

from the low and high temperature region respectively, one can estimate n_{rigid}:

$$n_{\text{rigid}}(T) = \frac{d(T) - d_{\text{fluid}}(T)}{d_{\text{rigid}}(T) - d_{\text{fluid}}(T)} \tag{24}$$

where $d(T)$ is the experimentally measured density of the glassformer.

The result for $n_{\text{rigid}}(T)$ of ZBLAN20 is presented in figure 9 as a function of temperature. We have used the data by Hasz *et al* [3] on ZBLAN20's conductivity and density. Unfortunately, while the conductivity, which varies in orders, can be measured with precision, the density, which varies by 20% only, is measured relatively less accurately. The agreement of n_{sol} obtained from conductivity and density data confirms the physical meaningfulness of equations (23) and (24) and justifies the validity of equation (4).

5. Conclusions

We have found that for all the investigated regular structures (2D and 3D composites, two and three component composites, isotropic and anisotropic composites, composites with equal and different concentrations of components) there is a domain of a universal behaviour of the effective conductivity. This domain can be qualitatively characterized as a range of 'low contrast' of the partial conductivities. For this domain of universality we have suggested an equation which gives a good approximation to the effective conductivity. Analysing the experimental data on ZBLAN20 conductivity and density, we have found that the suggested equation is valid for the random composites as well.

Acknowledgments

References

[1] Machavariani V Sh and Voronel A 2000 *Phys. Rev.* E **61** 2121
[2] Fel L G, Machavariani V Sh and Bergman D J 2000 *J. Phys. A: Math. Gen.* **33** 6669
[3] Hasz W C, Whang J H and Moynihan C T 1993 *J. Non-Cryst. Solids* **161** 127
[4] Dykhne A M 1970 *Sov. Phys.–JETP* **32** 63
[5] Tortet L, Gavarri J R, Musso J, Nihoul G, Clerc G P, Lagarkov A N and Sarychev A K 1998 *Phys. Rev.* B **58** 5390
[6] Keller J B 1964 *J. Math. Phys.* **5** 548
[7] Söderberg M and Grimvall G 1983 *J. Phys. C: Solid State Phys.* **16** 1085
[8] Schulgasser K 1976 *J. Math. Phys.* **17** 376
[9] Ghosh S S and Dasgupta C 1996 *Phys. Rev. Lett.* **77** 1310
    Kob W, Donati C, Plimpton S J, Poole P H and Glotzer S C 1997 *Phys. Rev. Lett.* **79** 2827
    Stillinger F 1988 *J. Chem. Phys.* **89** 6461
    Stillinger F and Hodgdon J 1994 *Phys. Rev.* E **50** 2064
    Kirkpatrick T, Thirumalai D and Wolynes P 1989 *Phys. Rev.* A **40** 1045
    Chamberlin R and Kingsbury D 1994 *J. Non-Cryst. Solids* **172–174** 318
    Bendler J and Schlesinger M 1992 *J. Phys. Chem.* **96** 3970
    Kivelson S, Zhao X, Kivelson D, Fisher T and Knobler C 1994 *J. Chem. Phys.* **101** 2391
[10] Gerharz B, Meier G and Fisher E 1990 *J. Chem. Phys.* **92** 7110
    Fisher E, Donth E and Steffen W 1992 *Phys. Rev. Lett.* **68** 2344
    Patterson G and Stevens J 1994 *J. Non-Cryst. Solids* **172–174** 311

Steffen W, Patkowsky A, Meyer G and Fisher E W 1992 *J. Chem. Phys.* **96** 4171

[11] Cicerone M and Ediger M 1993 *J. Phys. Chem.* **97** 10 489
Cicerone M, Blackburn F and Ediger M 1995 *J. Chem. Phys.* **102** 471
Earl K, Moscicki J, Polimeno A and Freed J 1997 *J. Chem. Phys.* **106** 9996
Sen S and Stebbins J F 1998 *Phys. Rev.* B **58** 8379

[12] Voronel A, Veliyulin E, Machavariani V Sh, Kisliuk A and Quitmann D 1998 *Phys. Rev. Lett.* **80** 2630

[13] Veliyulin E, Voronel A and Oye H A 1995 *J. Phys.: Condens. Matter* **7** 4821
Voronel A, Veliyulin E, Grande T and Oye H A 1997 *J. Phys.: Condens. Matter* **9** L247